Nanocarbon–Ionic Liquid Composites

DOI: 10.1002/ange.201408201

Entrapping an Ionic Liquid with Nanocarbon: The Formation of a Tailorable and Functional Surface**

*Yuxiao Ding, Xiaoyan Sun, Liyun Zhang, Shanjun Mao, Zailai Xie, Zhong-Wen Liu, and Dang Sheng Su**

Abstract: *An interface microenvironment between nanocarbon and ionic liquids (ILs) is presented. By an entrapping effect, a few layers of ILs can be finely deposited on the surface of nanocarbon, endowing amazingly tailorable surface properties. The entrapped IL layer, which was believed to be unable to be charred under pyrolysis conditions alone, can be further carbonized to a functional carbon layer. C, B, and N were confirmed to share the same hexagonal ring in the resultant layer, which provides more designable electronic properties.*

Recently, directly synthesized carbon materials from ionic liquids (ILs) have represented a burgeoning direction for the generation of functional carbon materials. The key advantage of ILs derived carbons is that by selection of task-specific ionic liquids, heteroatoms (such as N, B, P) can be easily incorporated into carbon frameworks, where the dopant is homogeneously distributed over the entire bulk.[1] However, many of ILs ultimately decompose to volatile components at elevated temperature, leading to very low carbon yields. Furthermore, ILs without metal or cross-linkable groups such as the cyano group[1c,e] are not likely to form carbonaceous material directly, while ILs with cross-linkable groups always suffer from the sacrificial use of hard templates.[2] Moreover, the usage of ionic liquids as carbon precursors is accompanied with relatively high costs, as compared to the low price of most other carbon precursors.

Our strategy to overcome all of these difficulties is to use the special interaction between ILs and graphitic carbon surface to disperse or coat ILs on nanocarbon support. The static-assistant CH–π interaction between ILs and graphitic support allows the entrapping and directing of ILs and modifies their thermal behavior. Coating with only a few layers of ILs on carbon nanotubes (CNTs) or graphene leads to a preparation of nanocarbon with a heteroatom-rich and functional surface. The method is simple and cost-effective, as a small amout of ILs is used. Model IL (alkylimidazolium tetrafluoroborate, without cross-linkable groups) acts as heteroatom donors and surface carbon precursors, while CNTs or graphene acts as model carbon skeleton. The IL precursors were first coated on the nanocarbon surface to form IL/nanocarbon gel.[3] Based on the volatility[4] of ILs under vacuum condition, the coating thickness on nanocarbon surface can be controlled by vaporing ILs.[5] The obtained IL/carbon nanocomposites were subsequently heat-treated to form a carbonaceous surface (named as NBC*x* or NBG*x*; *x* represents annealing temperatures) with tailorable heteroatom content (Scheme 1).

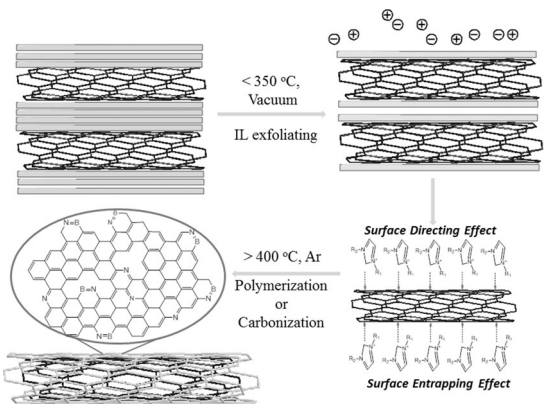

Scheme 1. Evolution process of the surface structures: from condensed IL ion pairs to polymeric structures, then to the graphitic structures.

High-resolution transmission electron microscopy (HRTEM) was used to compare the pristine CNT and the newly formed surface. The HHT (a type of MWCNTs treated at 3000 °C with a very high graphitization degree to exclude the influence of metal impurities, defects, and oxygen functional groups; Figure 1a) exhibits a very smooth outer layer, while the layer of IL can be observed on the surface of HHT forming a IL/HHT nanocomposite (Figure 1b) with a clear boundary between the IL precursor and HHT. This demonstrates that the physical evaporation process under low temperature has no obvious influence on the interaction between the IL and CNT. However, when annealing at 400 °C for one hour, the IL decomposed and polymerized to polymeric structures (NBC400). From Figure 1c, it can be

[*] Y. Ding, X. Sun, L. Zhang, S. Mao, Prof. D. S. Su
Shenyang National Laboratory for Materials Science
Institute of Metal Research, Chinese Academy of Sciences
72 Wenhua Road, Shenyang 110016 (China)
E-mail: dssu@imr.ac.cn
Dr. Z. Xie, Prof. D. S. Su
Fritz-Haber-Institut der Max-Planck-Gesellschaft
Faradayweg 4–6, 14195 Berlin (Germany)
Prof. Z. Liu
Key Laboratory of Applied Surface and Colloid Chemistry (MOE)
Shaanxi Normal University, Xi'an 710062 (China)

[**] The authors acknowledge financial support from MOST (2011CBA00504), the NSFC of China (21133010, 51221264, 21261160487), and the "Strategic Priority Research Program" of the Chinese Academy of Sciences, grant XDA09030103.

Supporting information for this article is available on the WWW under http://dx.doi.org/10.1002/anie.201408201.

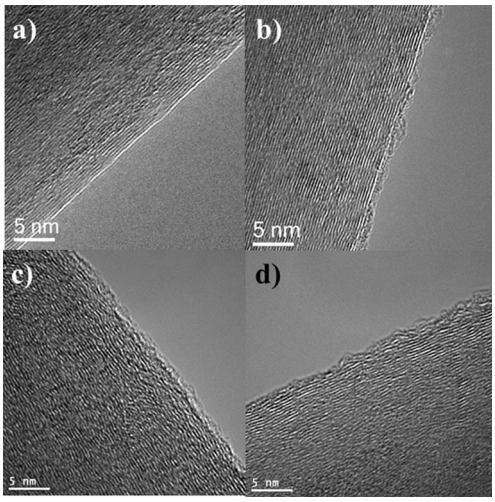

Figure 1. High-resolution TEM images of a) pristine HHT, b) IL/HHT nanocomposite, c) NBC400, and d) NBC500.

seen that the coating layer became thinner, more uniform, and compact. Although the difference of the polymer-like layer and HHT can be distinguished, the boundary between them seems to disappear. This might be caused by the decomposition of IL: the decomposed IL debris were tightly entrapped on the highly graphitic HHT surface and merged together. This means that graphitic surface has a potential as a trapping agent for the decomposed debris, explaining why the IL without cross-linkable groups can form carbonaceous materials on the CNT surface. With an increase of annealing temperature to 500 °C, the coating layer turns to a single graphitic layer (Figure 1 d). Furthermore, the rough surface indicates that the newly formed layer is abundant in defects. However, the graphitic fragments on the carbon surface are continuous.

Temperature-programmed desorption (TPD) of IL/HHT nanocomposites was used to study the evolution of IL. The signals of alkyl debris show a vertical decrease to the base line (as marked by dotted line at 425.3 °C in the Supporting Information, Figure S1) when the curves reach a maximum. This indicates that decomposition of IL is complete at 425 °C. The remaining fragments are entrapped by the nanocarbon skeleton forming carbonaceous polymer. Note that a series of shoulder peaks can be observed at about 400 °C, which is most likely due to the increasing entrapping force of HHT on IL layer by layer (one shoulder corresponds to one layer). The N and F elements during the heat treatment can be detected as N_2 and F^- in the mass spectra. Compared to the alkyl debris, they show more symmetric peaks (Supporting Information, Figure S1). After the main decompositions (as marked by dotted line at 431 and 450 °C for N and F, respectively), there is still a slight mass loss for both elements, which can be attributed to their overflow during the carbonization process. In the isothermal thermogravimetric analysis (TG) curves of pure IL (Supporting Information, Figure S1d), it can be observed that IL is lost totally within 10 min after maintaining a temperature of 400 °C. This indicates that the pure IL cannot form carbonaceous materials without being entrapped on a graphitic surface. Theoretical calculations suggest an interaction energy of $-275.9\ kJ\,mol^{-1}$ (Supporting Information, Figure S2 and Table S1) between the IL cation and the graphitic surface. Such a strong interaction energy indicates that the graphitic surface can entrap the IL debris when the IL is decomposed at high temperature.[6] The entrapped debris can then cross-link forming continuous graphitic fragments. Based on the TEM and TPD results, herein we propose a possible carbonization mechanism of the IL without cross-linkable functional groups (Supporting Information, Figure S3).

N and B heteroatoms are totally exposed on the NBC surface. Table S2 shows the N, B content obtained by XPS, which can be tailored by changing the annealing temperature. Note that the XPS detection depth can reach several nanometers, the surface available heteroatoms are obviously higher than the data given. The deconvolution results of B 1s in Figure 2 a reveal the evolution process of the B element with increasing temperature and agree with the formation of the single B species (N–B bond) in the obtained NBC900 surface. The deconvolution results of the N 1s (Supporting Information, Figure S4) can also confirm that the B, N, and C share the same hexagonal ring. With the evolution process of N and B, the obtained carbon surface can provide designable electronic properties. Electron energy-loss spectroscopy (EELS) was used to identify the bonding environment of the C, N, and B.[7] The EELS K-edge spectrum of the resultant NBG400 is shown in the Supporting Information, Figure S5. Figure S5 a shows the carbon K-edge in which line 1 marks the center of the $1s\rightarrow\pi^*$ transitions in graphene (285.3 eV), and line 2 marks the onset of the $1s\rightarrow\sigma^*$ transitions in graphene (291.7 eV).[8] The π^* peak of the boron K-edge observed at 192.5 eV (Figure S5 b) indicates that boron atoms are sp^2-hybridized, like their carbon counterparts.[9] The π^* peak of the nitrogen K-edge (Figure S5 c) indicates that nitrogen atoms are in the sp^2-hybridized structure as well.[9] The XPS and EELS verify the supposed carbonization process in the Supporting Information, Figure S3.

Figure 2 b shows the Raman spectra and their deconvolution peaks of pristine CNTs and NBC samples. The deconvoluted peaks can be attributed to ionic impurities at about $1200\ cm^{-1}$ (D4 peak), graphene layer edges at about $1330\ cm^{-1}$ (D1 peak), amorphous carbon at about $1500\ cm^{-1}$ (D3 peak), ideal graphitic lattice at about $1565\ cm^{-1}$ (G peak) and disordered graphitic lattice of surface graphene layers at about $1600\ cm^{-1}$ (D2 peak).[10] With the increase of the annealing temperature, the intensity of disordered graphitic lattice increased. The I_D/I_G (D1) values of HHT, NBC400, and NBC500 are 0.50, 0.75, and 1.11, respectively. This demonstrates that the formed graphitic lattice was tightly adsorbed onto HHT by π–π stacking. Obviously, a high temperature (500 °C, I_D/I_G 1.11) favors the formation of the new rough graphitic surface than a low temperature (400 °C, I_D/I_G 0.75). This is in agreement with the TEM study, which reveals that more carbonaceous polymeric structures were formed at 400 °C (Figure 1 c). The D1 peak represents the dissociative disordered graphitic lattice on the surface. With the formation of the new surface, the dissociative graphitic fragments

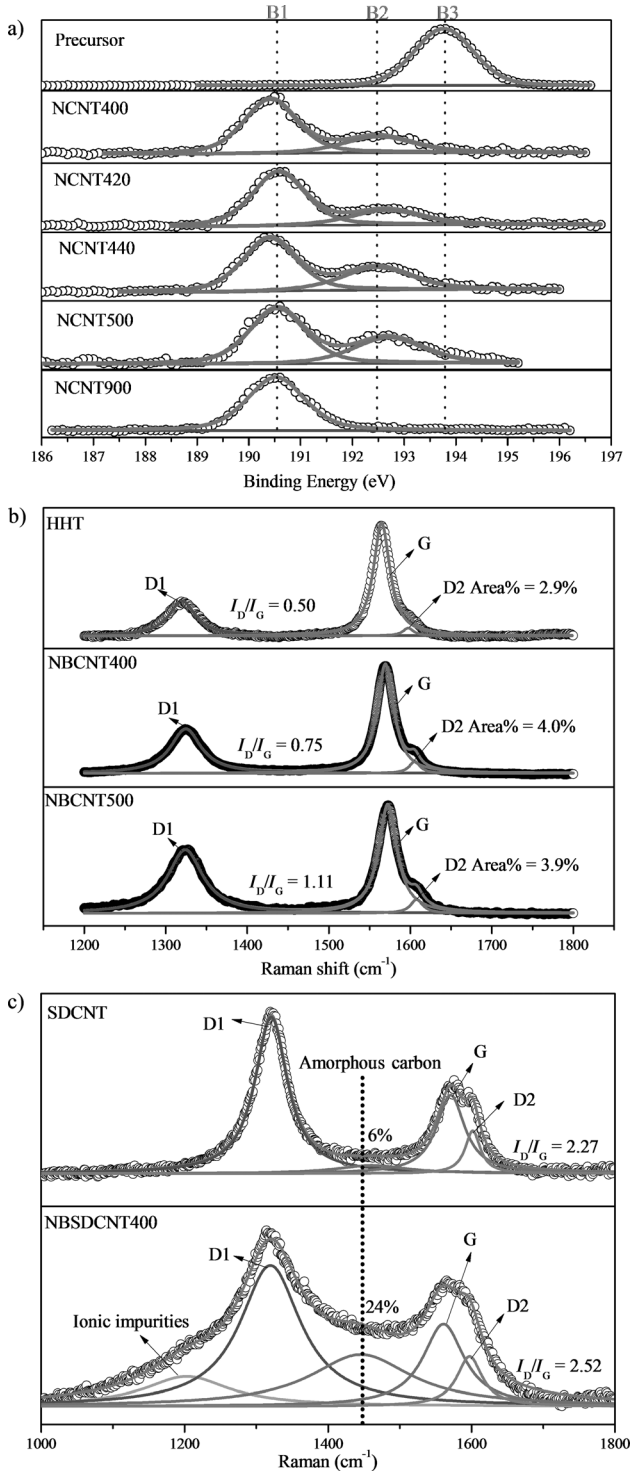

Figure 2. a) B 1s XPS spectra and distribution diagrams of different samples from IL/HHT precursors. The fitting is performed by fixing the peak maximum within ±0.1 eV for all of the spectra and applying a full-width half-maximum (FWHM) of 1.2–1.6 eV. b) Raman spectra of pristine HHT, NBC400, and NBC500 upon excitation at 633 nm and their deconvolution results. c) Raman spectra of pristine SDCNT, NBSDC400, and their deconvolution results. The two series of samples were obtained following the same synthesis process.

increase as well (area % from 2.9 % to about 4.0 %). Since the highly graphitic HHT surface has a static-assistant CH–π hydrogen bond with IL precursor,[5] how can the amorphous carbon on nanocarbon surface affect the carbonization process? To probe this question, we have used a type of CNT (SDCNT) with about 6 % amorphous carbon (area % from Raman spectrum with deconvolution) for our study. From the deconvolution of Raman spectra (Figure 2 c), not only an increase in disordered graphitic lattice of NBSDC400 is observed (from 2.27 to 2.52), but also the amount of amorphous carbon shows a remarkable increase from 6 % to 24 %. As there is no amorphous carbon formed on HHT surface, this result clearly indicates that the surface condition of CNT shows a directional induction for the cross-linking process of IL precursors. The imidazolium cation of the IL can stay on the graphitic carbon surface in a specific angle (Supporting Information, Figure S2). When a large amount of ILs is used, the graphitic carbon surface will show a directing effect, where the ILs can arrange above the hexagonal ring of graphitic structure. For a highly graphitic surface, it shows a highly ordered directing; while for a rough graphitic surface, it shows a scruffy directing of the ILs. The directing effect can thus be used to form carbon with different degree of order. Note that the rough surface of the SDCNT leads to an introduction of ionic impurities on the NBSDC400 surface, which is probably caused by the tight encapsulation of the decomposed ionic debris between the newly formed amorphous carbon and the CNT surface.

XRD patterns of NBC (Supporting Information, Figure S6) show some interesting features. Compared to the pristine HHT, the broad diffraction peak centered at $2\theta = 24°$ of IL/HHT nanocomposites exhibits an amorphous form of the IL solidification. After annealing at 400 °C, the formed polymeric structures on the surface cause a series of diffraction peaks marked by asterisk. These peaks disappeared in NBC500, indicating a transition from a polymeric to graphitic structure. Both NBC400 and NBC500 show a peak with *d* spacing about 7.6 Å, which might be attributed to the formation of micropore with short-range ordering, indicating a directional influence[3a,11] of the graphitic structure to the carbonization process of IL precursors without cross-linkable functional groups.

The resulting carbonaceous coating layers at different temperatures render nanocarbon with different surface properties. Figure 3 a,b show water droplet shapes over pristine HHT and NBC400. HHT is super-hydrophobic with a contact angle of 150.4°, while NBC400 is totally hydrophilic with a contact angle of 26.1°, which may be caused by the short carbon chains of the polymer-like surface forming hydrogen bonds with water. When graphene is used instead of CNTs to make the composition, the same hydrophility was observed (Supporting Information, Figure S7). This indicates that the formed coating layer covers the nanocarbon graphitic surface uniformly and totally determines the surface properties of the nanocomposite. With the increase of the annealing temperature, the newly formed graphitic layers become thinner, so the proportion of exposed heteroatoms becomes higher, implying the change of surface chemistry. As shown in Figure 3 c, with the introduction of the IL-based coating, the zeta potentials varies from 0 to −34 mV (pH = 7). The adjustable range of the surface potential undoubtedly pro-

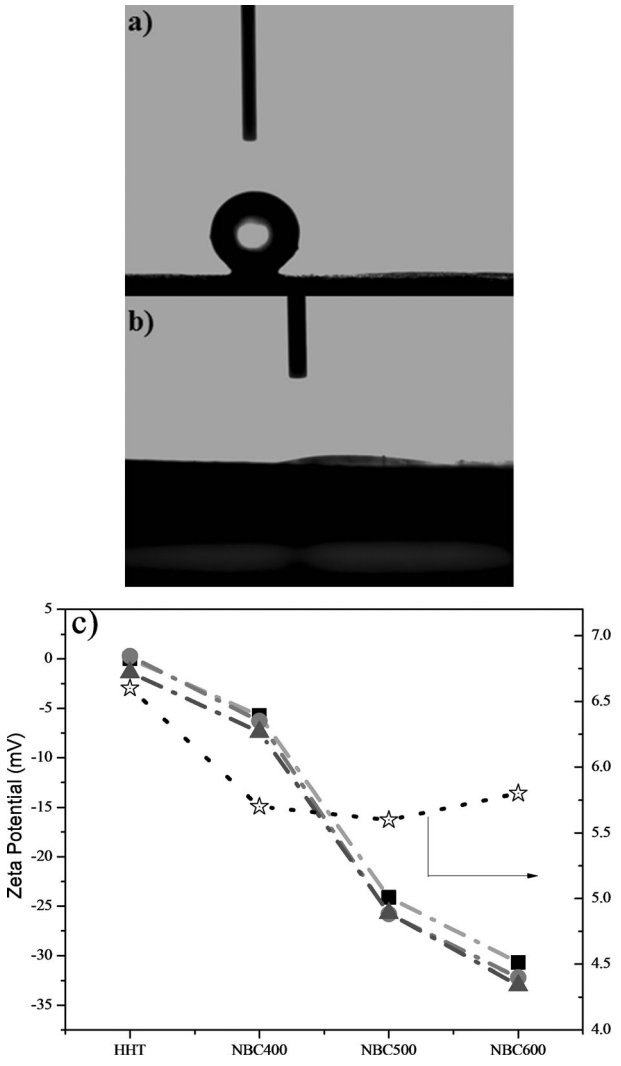

Figure 3. Water droplet shape over a) HHT and b) NBC400, revealing a contact angle of 150.4° and 26.1°, respectively. c) Zeta potential of three repeated tests (■, ●, ▲) and PH data (⋆) of different CNT samples.

vides more choices for task-specific applications. Moreover, the obtained boron-containing coating surfaces of both the CNT and graphene series exhibit similar weak acidity (Figure 3c; Supporting Information, Table S3), which might be caused by the Lewis acidity of the graphitic boron atom. It is noted that carbon materials with Lewis acidity properties have seldom been reported.

In summary, the strong interaction between ILs and graphitic support allows the entrapping and directing of ILs on nanocarbon and thus the synthesis of heteroatoms-rich carbon materials with non-cross-linkable functional ILs. The structure of obtained surface can be tailored from condensed IL ion pairs to the polymeric, then to the graphitic structures. The properties of the formed nanocarbon surface, such as the hydrophobicity–hydrophility, surface potential, and acid–base character, can be easily tuned by changing the treatment conditions. Heteroatoms are fully exposed on the surface, rendering a high atomic effecting. A few layers and even single layer can be obtained on the surface. Moreover, the template removal process is not needed. All the above advantages bring not only an economical potential application of ILs, but also a fundamental understanding of the nanocarbon and IL interface. The numerous kinds of ILs will undoubtedly give extensive heteroatom candidates for the method.

Experimental Section

Catalyst preparation: The NBCNT was prepared as the following procedure: ILs ([Emim]BF_4, [Bmim]BF_4, or [Omim]BF_4, purchased from Alfa Aesar) and HHTs (a type of MWCNTs treated at 3000 °C with very high graphitization degree, which can remove the influence of metal impurities, defects, and oxygenic functional groups on CNT surface) were first mixed (mass ratio 10:1) and ultrasonically treated for 10 min to disperse the CNTs in the IL phase. As the precursors are liquids at room temperature, they can easily coat on CNT templates, avoiding any high-pressure techniques. Then the mixture was centrifuged at 9000 r min^{-1}. A transparent liquid phase, identified as pure IL, was recycled from a black lower gel phase containing both IL and CNTs. The black gel phase was moved to small quartz boats which were placed in the center of a larger alumina tube running through the center of a furnace. Temperature-programmed annealing processes were carried out according to the conditions: first step, vacuum condition, 5 °C min^{-1} from room temperature to 330 °C and maintaining for 50 min (IL/HHT nanocomposites); second step, argon condition (200 mL min^{-1}), 5 °C min^{-1} from room temperature to different temperatures and maintaining for 60 min. The final products (NBCNT) were obtained from the inside of the quartz boats after the annealing process. Graphene (purchased from the sixth element Changzhou Ltd) and SDCNT (purchased from CNano Technology Ltd) were used to form N and B co-doped nanocarbon with [Bmim]BF_4 in the same way of NBCNT400.

Characterization: The images of high-resolution TEM and EELS were observed on a Tecnai G2 F20 S-TWIN operated at 200 kV and a Philips CM200 FEG operated at 200 kV. Temperature-programmed desorption (TPD) was performed on a tube furnace and an AVI Omnistar mass spectrometer. The atmosphere was He and the heating rate was 5 °C min^{-1} from room temperature to 900 °C. Thermogravimetric (TG) was performed on NETZSCH STA 449 F3 under a flow of argon (50 mL min^{-1}) with a heating rate of 5 °C min^{-1} from 35 to 400 °C and maintaining for 2 h. XPS characterization was performed on an ESCALAB 250 instrument with $Al_{K\alpha}$ X-rays (1489.6 eV). Raman spectroscopy was conducted with a LabRam HR 800 spectrometer using a 633 nm excitation at 25 mW laser power with a 2.5 cm^{-1} resolution. X-ray diffraction (XRD) measurements were performed on a D/max 2400 diffractometer (JEOL Ltd., Japan) at a scanning rate of 1° min^{-1}, with graphite monochromatized $Cu_{K\alpha}$ radiation ($l = 0.1506$ nm). Zeta potentials and the PH values of the pristine CNTs, graphene, and different samples were measured by a Malvern zeta meter (Zetasizer 2000). The sample solution was 0.1 M sodium chlorate solution at 25 °C.

Received: August 13, 2014
Revised: October 8, 2014
Published online: November 4, 2014

Keywords: interfaces · ionic liquids · nanocarbons · nanocomposites · surface modification

[1] a) T.-P. Fellinger, A. Thomas, J. Yuan, M. Antonietti, *Adv. Mater.* **2013**, *25*, 5838 – 5855; b) J. S. Lee, X. Wang, H. Luo, G. A. Baker, S. Dai, *J. Am. Chem. Soc.* **2009**, *131*, 4596 – 4597; c) J. S. Lee, X. Wang, H. Luo, S. Dai, *Adv. Mater.* **2010**, *22*, 1004 – 1007; d) J. P.

Paraknowitsch, J. Zhang, D. Su, A. Thomas, M. Antonietti, *Adv. Mater.* **2010**, *22*, 87 – 92; e) W. Yang, T.-P. Fellinger, M. Antonietti, *J. Am. Chem. Soc.* **2011**, *133*, 206 – 209.

[2] a) A. Chen, Y. Yu, H. Lv, Y. Wang, S. Shen, Y. Hu, B. Li, Y. Zhang, J. Zhang, *J. Mater. Chem. A* **2013**, *1*, 1045 – 1047; b) T.-P. Fellinger, F. Hasché, P. Strasser, M. Antonietti, *J. Am. Chem. Soc.* **2012**, *134*, 4072 – 4075.

[3] a) T. Fukushima, A. Kosaka, Y. Ishimura, T. Yamamoto, T. Takigawa, N. Ishii, T. Aida, *Science* **2003**, *300*, 2072 – 2074; b) J. Lee, T. Aida, *Chem. Commun.* **2011**, *47*, 6757 – 6762.

[4] a) M. J. Earle, J. Esperanca, M. A. Gilea, J. N. C. Lopes, L. P. N. Rebelo, J. W. Magee, K. R. Seddon, J. A. Widegren, *Nature* **2006**, *439*, 831 – 834; b) P. Wasserscheid, *Nature* **2006**, *439*, 797 – 797.

[5] Y. Ding, D. S. Su, *ChemSusChem* **2014**, *7*, 1542 – 1546.

[6] a) R. Göbel, R. J. White, M. M. Titiricib, A. Taubert, *Phys. Chem. Chem. Phys.* **2012**, *14*, 5992 – 5997; b) S. M. Chen, G. Z. Wu, M. L. Sha, S. R. Huang, *J. Am. Chem. Soc.* **2007**, *129*, 2416 – 2417.

[7] R. J. Nicholls, Z. Aslam, M. C. Sarahan, A. Koós, J. R. Yates, P. D. Nellist, N. Grobert, *ACS Nano* **2012**, *6*, 7800 – 7805.

[8] S. Waidmann, M. Knupfer, J. Fink, B. Kleinsorge, J. Robertson, *Diamond Relat. Mater.* **2000**, *9*, 722 – 727.

[9] J. M. Lee, J. S. Park, S. H. Lee, H. Kim, S. Yoo, S. O. Kim, *Adv. Mater.* **2011**, *23*, 629 – 633.

[10] a) A. Cuesta, P. Dhamelincourt, J. Laureyns, A. Martinezalonso, J. M. D. Tascon, *Carbon* **1994**, *32*, 1523 – 1532; b) B. Dippel, H. Jander, J. Heintzenberg, *Phys. Chem. Chem. Phys.* **1999**, *1*, 4707 – 4712; c) T. Jawhari, A. Roid, J. Casado, *Carbon* **1995**, *33*, 1561 – 1565; d) F. Tuinstra, J. L. Koenig, *J. Chem. Phys.* **1970**, *53*, 1126 – 1130; e) Y. Wang, D. C. Alsmeyer, R. L. Mccreery, *Chem. Mater.* **1990**, *2*, 557 – 563.

[11] J. J. Lee, A. Yamaguchi, M. A. Alam, Y. Yamamoto, T. Fukushima, K. Kato, M. Takata, N. Fujita, T. Aida, *Angew. Chem. Int. Ed.* **2012**, *51*, 8490 – 8494; *Angew. Chem.* **2012**, *124*, 8618 – 8622.

